Lipid Membrane Flexibility in Protic Ionic Liquids

Supplementary Information

Shurui Miao[1], Ingo Hoffmann[2], Michael Gradzielski[3], Gregory Warr[1*]

[1] School of Chemistry and University of Sydney Nano Institute, The University of Sydney, NSW 2006, Australia

[2] Institut Max von Laue-Paul Langevin (ILL), 71 avenue des Martyrs, CS 20156, Cedex 9, F-38042 Grenoble, France.

[3] Stranski-Laboratorium für Physikalische und Theoretische Chemie, Institut für Chemie, Straße des 17. Juni 124, Sekr. TC7, Technische Universität Berlin, D-10623 Berlin, Germany

Experimental Method

Partially deuterated ionic liquids were produced by neutralising formic acid with D_5-ethylamine (98%, Cambridge Isotope) or D_4-ethanolamine (98%, Cambridge Isotope) in dilute D_2O solutions (~ 20 wt% amine). The end point was determined through pH measurement (pH = 6). The resultant solution was gently dried on rotary evaporator at 40 ˚C and 50 mbar for 10 minutes. As both alkylamine and formic acid are volatile species prone to evaporation under high vacuum (i.e. both EAF and EtAF have high vapour pressure relative to other PILs), further drying was performed by bubbling dry N_2 gas through the sample for more than 7 days. Identical procedures were carried out with hydrogenous materials and the stoichiometry after drying was confirmed by 300 MHz ^{1}H NMR. Both D_8-EAF and D_8-EtAF are clear, room-temperature liquids with water contents <1 wt%, determined using Karl-Fischer Titration (Metrohm 784 KFP Titrino).

Egg lecithin powder (> 99%, Sigma) was used to prepare 1 %w/v unilamellar vesicle by the ethanol injection method. The required mass of lipid was dissolved in ethanol at 60 ˚C to yield a 40 mM solution, which was then slowly injected into the IL (60 ˚C) through a 21 G needle under vigorous stirring. Ethanol was fully removed using a rotatory evaporator while monitoring the total mass of the mixture. However, due to the presence of an azeotrope between ethanol and water, we expect some ethanol residue (< 5 mg) remain in the D_2O sample. The presence of large aggregates on the scale of 10^2 nm was confirmed using bench-top light and x-ray scattering.

The vesicle samples were examined in detail by small angle neutron scattering at Institut Max von Laue-Paul Langevin (ILL) and Australian Centre for Neutron Scattering (ACNS). Scattering at wave vectors between 0.002 – 0.5 Å^{-1} were collected at 25 ˚C for vesicles in D_8-EAF, D_8-EtAF and D_2O (on the D11 beamline at the ILL: sample-detector distances at 5.5, 8 and 40.5 m; neutron wavelength = 5.5 Å with FWHM = 9% and a sample-aperture of 15 mm in diameter is used),[1] and for vesicles in D_8-EAF + 50 wt% D_2O, D_8-EtAF + 50 wt% D_2O and D_2O (on the QUOKKA beamline at the ACNS: sample-detector distances at 4, 8 and 20m, neutron wavelength = 6 Å, beam divergence = 10% and a sample-aperture of 30 mm in diameter is used).[2] Samples of vesicles in PIL-water mixtures were recycled from NSE measurements and aged for 3 months; other samples in pure solvents were freshly prepared within a week of the scattering experiment. Isotropic two-dimensional scattering patterns were reduced to I(Q) using modified NIST routines in Igor™. The first set of SANS at ILL confirmed that the prepared vesicle samples were suitable for the subsequent neutron spin echo measurement. Both sets of SANS patterns were analysed using the Kratky-Porod method to determine bilayer thickness.

Neutron spin echo (NSE) spectra were collected on the IN15 beamline at the ILL.[3] Measurements were performed with three detector configurations at 25 ˚C (the corresponding longest Fourier times are given in parentheses), namely neutron wavelength of 17 Å (952 ns) at detector angles of 5° and 8° and a wavelength of 13.5 Å (477 ns) at

a detector angle of 9°; covering a q-range from 0.026 $Å^{-1}$ to 0.081 $Å^{-1}$ with three q values per configuration. Due to the high viscosity of solvent, accessing long Fourier times is necessary. On average, 8 to 10 hours of acquisition was accumulated per sample. The scattering intensity was reduced by dividing resolution and subtracting the solvent signal, yielding the intermediate scattering functions which were fitted to an exponential decay. The data were analysed using the Zilman-Granek model to understand membrane flexibility.

Dynamic light scattering (DLS) measurements were also obtained simultaneously through an in-line DLS attached to IN15. A He-Ne laser of 632.8 nm at a fixed angle of 90˚ to the sample was used. The signal was detected by 2 Excelitas SPCM AQRH-13 APD detectors and the correlation function was calculated by a Flex02-01 digital correlator in pseudo-cross correlation to eliminate artefacts at short correlation times from after pulsing of the detectors. The apparatus was calibrated to 195 nm latex particles and data analysis was done by fitting a stretched-exponential decay function, followed by the application of the Stoke-Einstein equation of Brownian motions.

In both DLS and NSE analysis, the viscosities of solvents were experimentally measured at 25 ˚C on an MCR 502 WESP Rheometer (Anton Paar) using corresponding hydrogenous ILs and their mixtures. Parallel-plate measuring system was used and the dynamic viscosity was measured between shear rates of 1 – 100 Hz.

Surface tensions of egg lecithin solutions in ILs were measured using the pendant drop method on a CAM200 (KSV instruments) goniometer at room temperature (22±1 ˚C). Samples with < 1 wt% lipid were prepared using a dilute lipid solution in dichloromethane (DCM, Analytical grade, Merck, no detectable impurities under gas chromatography). A small volume of DCM solution was transferred to a clean container, followed by evaporation of solvent using nitrogen gas. Deposited lipids were mixed with ILs and sonicated for 1 minute. Samples were vortexed for > 30 s to ensure that the vesicle dispersion was homogenous prior to loading for measurements. Due to the high viscosity of ILs, each droplet was equilibrated for >10 minutes under a nitrogen atmosphere, 1000 frames at 16 ms intervals were collected and among them 1 frame selected for analysis. Images thus obtained were fitted to the Young-Laplace equation to yield surface tensions. A minimum of 3 consistent measurements were collected for each system. Results are shown in Figure S7.

Dynamic light scattering (Nano-ZS Zetasizer (Malvern), at 25 ˚C) was utilised alongside surface tension measurements to detect the presence of vesicles. 1 wt% samples were prepared using the ethanol injection method, followed by serial dilution to produce samples at lower concentrations. Three independent measurements were performed on each sample. Results were used as a confirmation of the presence of lipid aggregates.

Confocal laser microscopy was performed at the Sydney Microscopy and Microanalysis facility by Dr Pamela Young. 0.1 wt% lipid dispersion (vesicles by sonication) with 0.1 µM Nile Red was used for analysis. Laser excitation using 560 nm and 488 nm were performed for emission and fluorescent lifetime imaging respectively, emission was collected for 575 to 625 nm.

NSE spectra and Fitting

Neutron spin-echo spectroscopy (NSE) directly measures the intermediate scattering function, $S(q,t) = I(q,t)/I(q,0)$.[4] Measurements were performed on the IN15 beamline at Institut Laue-Langevin in Grenoble, France. Since its recent upgrade, Fourier times (t) up to 1000 ns can be reached using neutrons with a wavelength of 17.3 Å thanks to a fourfold increase of the maximum field integral.[3]

Membranes undergo long wavelength undulation motions that can be described using the Zilman-Granek model.[5] The resulting intermediate scattering function is

$$S(q,t) = e^{-(t\Gamma q^3)^{\frac{2}{3}}} \quad [S1]$$

where Γ is the relaxation rate, and is related to the mean bending modulus κ through:[6-7]

$$\Gamma = 0.0069\gamma_k \left(\frac{k_B T}{\kappa}\right)^{\frac{1}{2}} \frac{k_B T}{\eta} \quad [S2]$$

with Boltzmann constant k_B, temperature T, solvent viscosity η and for $\kappa/k_B T >> 1$, $\gamma_k \sim 1$. This equation accounts for several features of lipid bilayers[4-6] including dissipation of viscosity in the membrane,[8-9] monolayer compressibility and lateral flow and friction of opposing monolayers within the bilayer.[10-12]

In addition, translational diffusion needs to be taken into account, which we do here simply by multiplying Eq. S1 by the expression for a diffusing particle to obtain

$$S(q,t) = e^{-Dtq^2} e^{-(t\Gamma q^3)^{\frac{2}{3}}} \quad [S3]$$

which describes a diffusing particle whose surface is fluctuating due to thermal energy, and where D is the translational diffusion coefficient. NSE data was fitted using Eq. S3 using a single value of Γ for all q (global fit) and D was taken from DLS measurements which were performed simultaneously using IN15's *in situ* DLS. Results are shown in Figure S1.

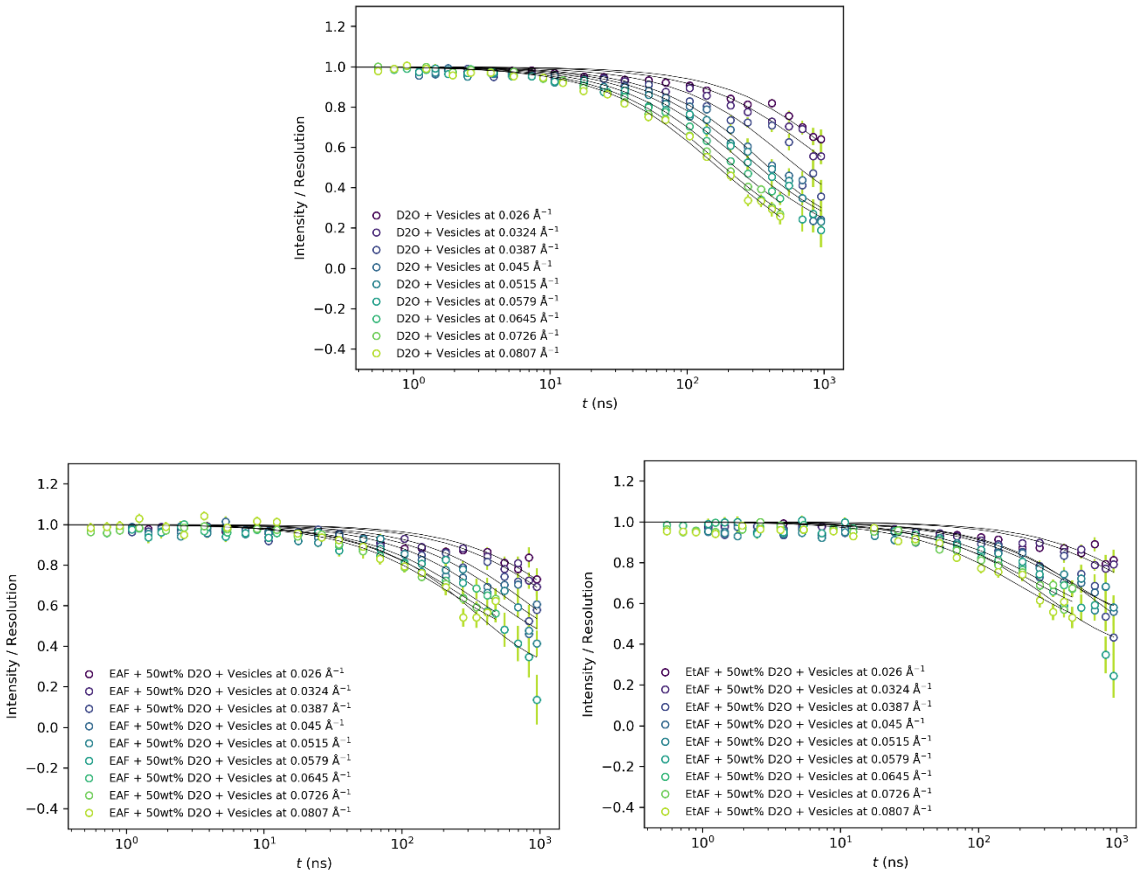

Figure S1. All NSE spectra with global fitting across all 9 q-values (solid lines). Continue to the next page.

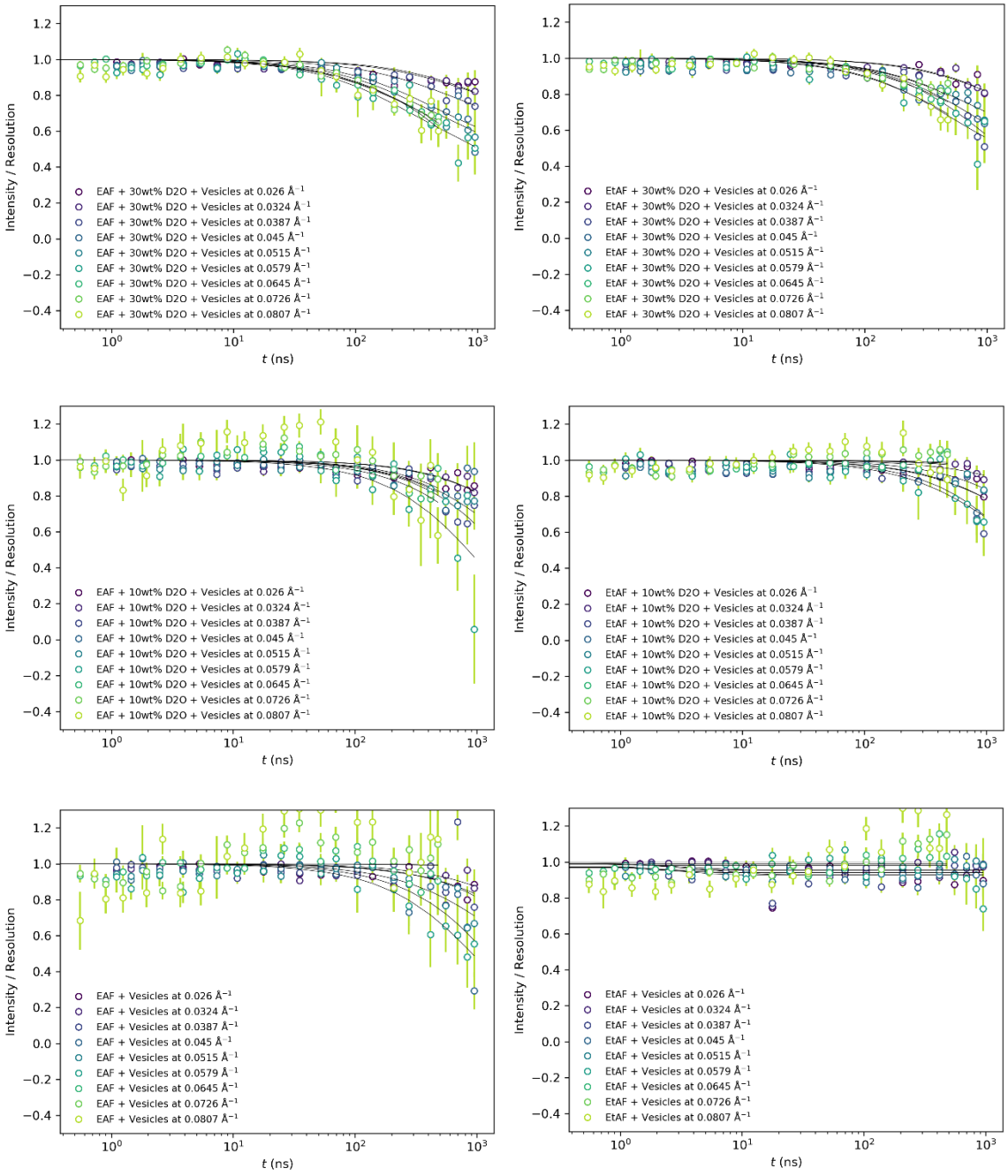

Figure S1. All NSE spectra with global fitting across all nine q-values (solid lines).

Figure S2 shows the experimental NSE spectra in water and the scaled (by viscosity) NSE spectra of EAF and EtAF when assuming identical behaviour as water (*i.e.*, same membrane flexibility). Within the experimental time range, all four scaled spectra are almost horizontal lines with negligible decay in intensity, which are extremely difficult to confirm considering experimental uncertainty. This is consistent with our experimental NSE spectra (Figure S1) of vesicles in both pure PILs, indicating the relaxation rate of undulation motions within PILs are equal or slower than vesicles in D_2O.

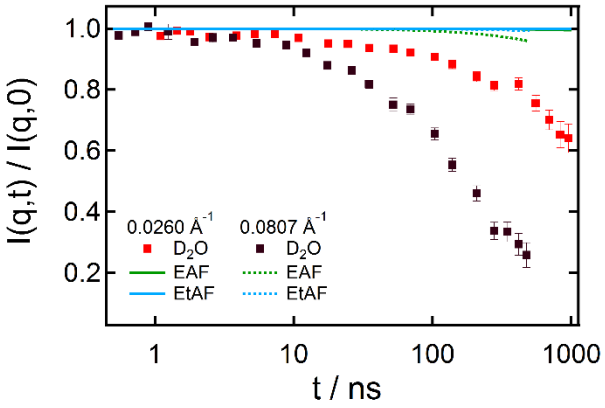

Figure S2. Experimental (markers) and scaled (lines) NSE spectra of vesicles in D_2O at the highest and lowest examined q-value. Scaling was done by assuming vesicles have the identical bending moduli as in D_2O but with experimental viscosities of EAF (green) and EtAF (Blue).

NSE Global Fit

The best fit of NSE was identified by the smallest chi-square value (of the global fit, using all of the acquired data) as shown in Figure S3 for EAF + 50 wt% D_2O, EtAF + 50 wt% D_2O and pure D_2O. An unambiguous minimum is observed within the physically meaningful range of relaxation rates (Γ).

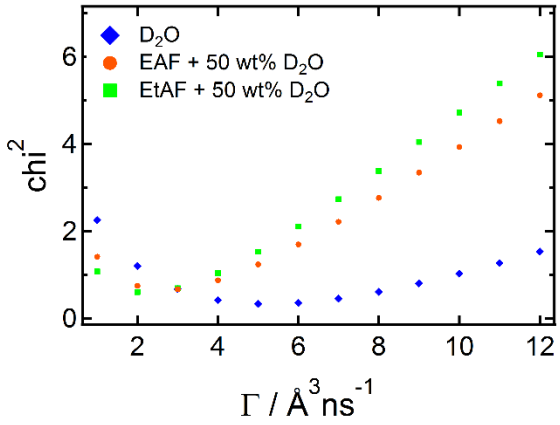

Figure S3. chi-square values of the global fit of selected NSE datasets versus relaxation rate (Γ). A clear minimum is present to yield a unique best fitting value of Γ.

DLS Measurements

DLS patterns shown in Figure S4 were accumulated throughout the NSE measurements. These were fitted to a stretched exponential model in order to extract the diffusion coefficient:

$$I(t) = Bkg + Ae^{-2(\Gamma t)^{\alpha}} \quad [S4]$$

where Γ is the relaxation rate and α is the stretching exponent, proportional to polydispersity. The diffusion coefficient (D) can be calculated from Γ using:

$$D = \frac{\Gamma}{q^2} \quad [S5]$$

where q correspond to a 90˚ scattering angle and the He-Ne laser wavelength of 632.8 nm, calibrated using 195 nm latex particles. The hydrodynamic radii of the vesicles, r_H, can then be determined from the diffusion coefficient by the Stokes-Einstein equation

$$D = \frac{RT}{N_A}\frac{1}{6\pi\eta r_H} \quad [S6]$$

Where R and N_A are the gas and Avogadro constants, respectively, T is temperature, and η is solvent viscosity.

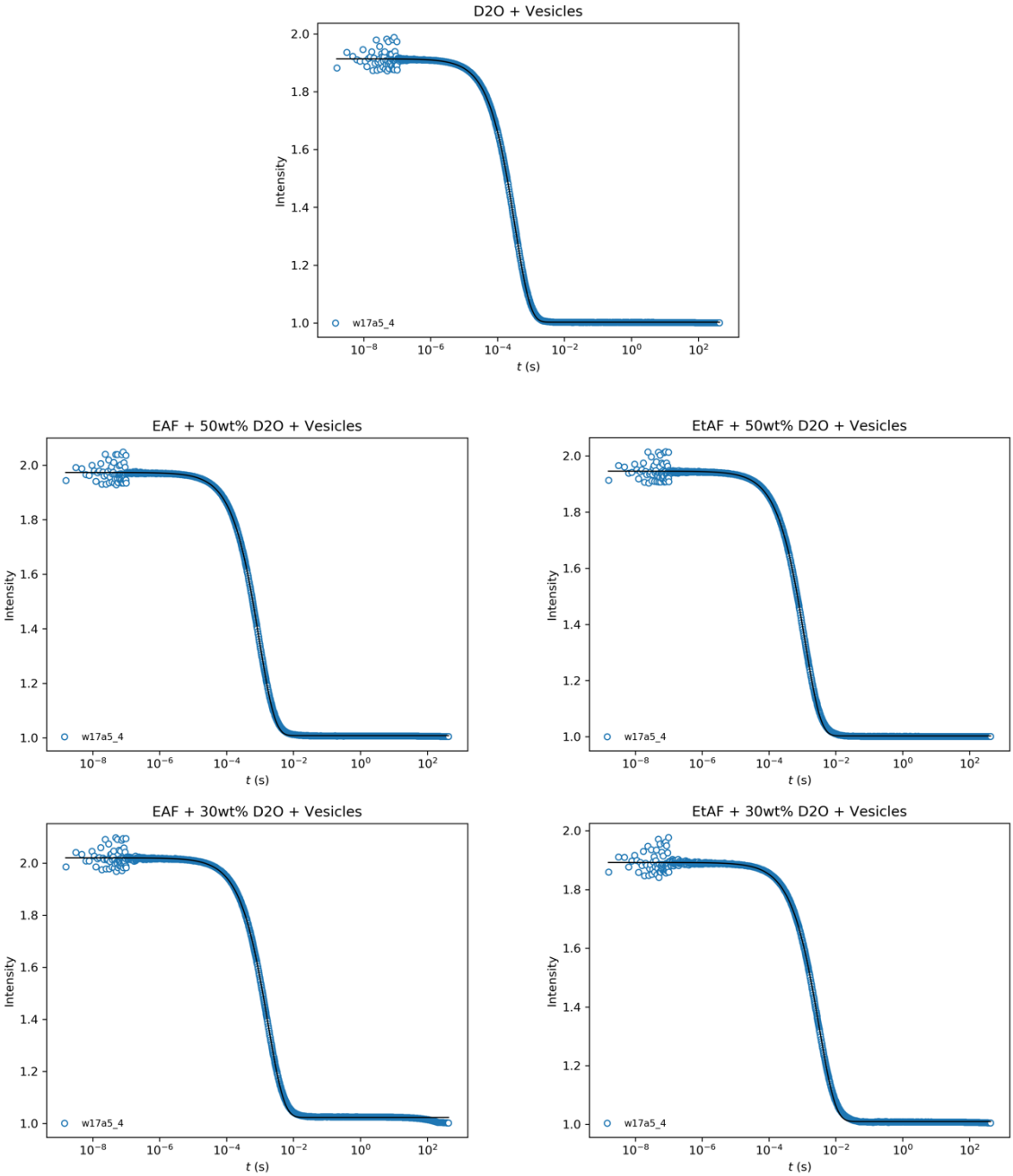

Figure S4. All DLS patterns with stretched-exponential fit (solid lines). Continue to the next page.

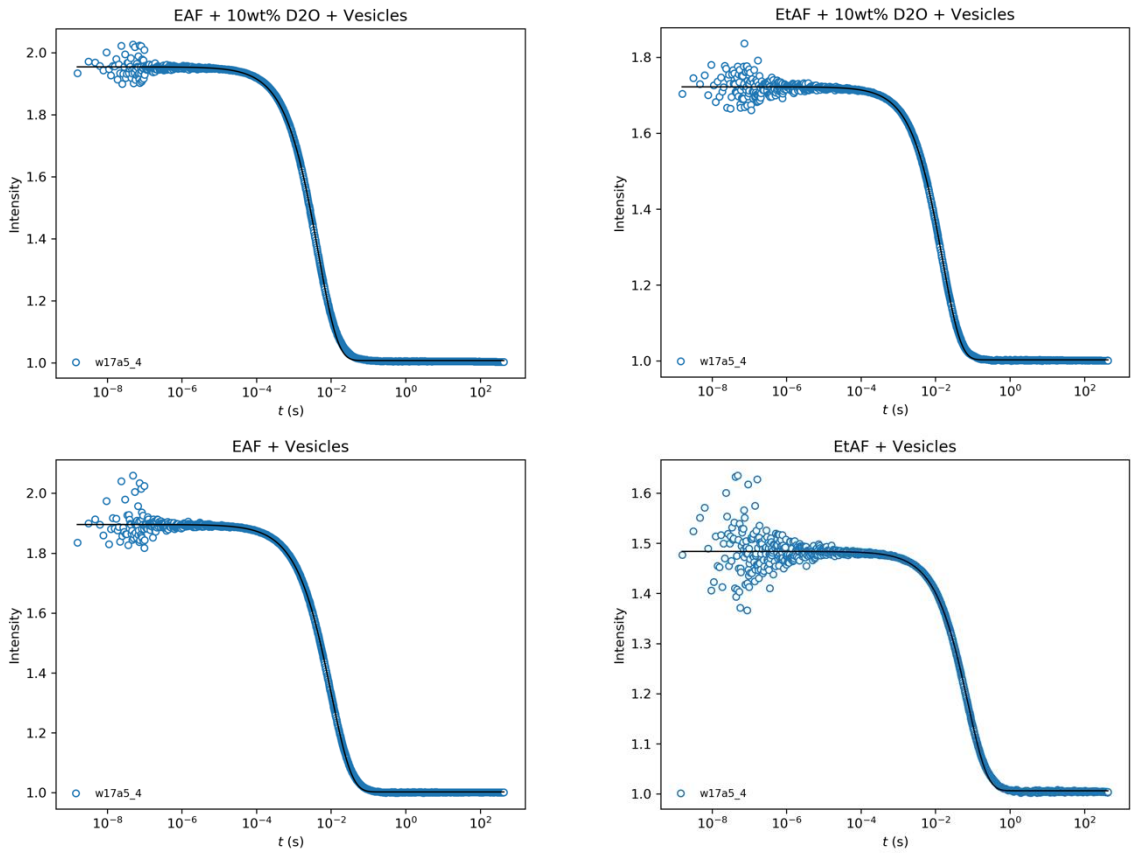

Figure S4. All DLS patterns with stretched-exponential fit (solid lines).

Table S1. The relaxation rate (Γ), hydrodynamic radius (r_H) and the stretching exponent (α) of fitted DLS.

Solvent	(Γ/S)	r_H (nm)	α
D_2O	1480 ± 10	89.7 ± 2.2	0.94
EAF + 50 wt% D_2O	501 ± 2	74.0 ± 1.0	0.92
EAF + 30 wt% D_2O	273 ± 1	62.8 ± 1.6	0.89
EAF + 10 wt% D_2O	99.2 ± 0.5	63.5 ± 1.6	0.83
EAF	43.6 ± 0.3	73.2 ± 1.8	0.79
EtAF + 50 wt% D_2O	409 ± 2	98.8 ± 3.1	0.91
EtAF + 30 wt% D_2O	146 ± 1	127 ± 3	0.89
EtAF + 10 wt% D_2O	29.7 ± 0.2	104 ± 3	0.88
EtAF	5.83 ± 0.11	127 ± 3	0.83

Kratky-Porod analysis of SANS:

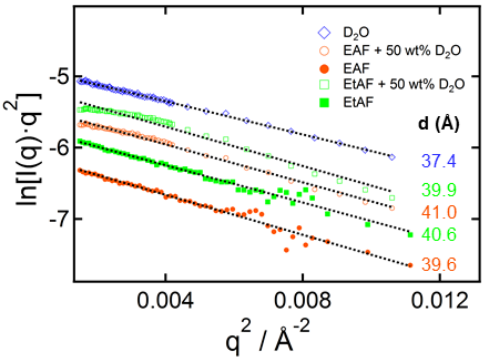

Figure S5. Kratky-Porod plot of experimental SANS data between 0.0015 Å^{-2} ≤ q^2 ≤ 0.011 Å^{-2} (corresponding to length scales between 60 and 160 Å), showing derived bilayer thicknesses (d). EAF (red), EtAF (green) and D_2O (blue). SANS patterns in filled markers were collected on D11 beamline, hollow markers were collected on QUOKKA beamline. IL + 50 wt% D_2O samples are 3 months old at the time of acquisition.

Kratky-Porod analysis of experimental SANS patterns yielded nearly parallel lines, corresponding to similar membrane thicknesses (*d*) in all solvent environments as shown in the Figure S5 and Figure 1a). Values are summarized in Table S2.

Table S2. Mean-square radius of gyration ($R_g{}^2$) and bilayer thickness (d) from Kratky-Porod analysis of SANS patterns.

Solvent	$R_g{}^2$ (Å^2)	d (Å)
D_2O	116 ± 1	37.4 ± 0.1
EAF + 50 wt% D_2O	133 ± 2	39.9 ± 0.2
EAF	140 ± 3	41.0 ± 0.5
EtAF + 50 wt% D_2O	138 ± 3	40.6 ± 0.5
EtAF	131 ± 3	39.6 ± 0.4

SANS Fits

SANS patterns were calculated using the unilamellar vesicle model in the SASview software package with homogeneous bilayer thickness (determined from Kratky-Porod analysis) and a fixed volume fraction of 1 vol%.[13] Pinhole collimation is used for SANS measurements therefore desmearing of the q resolution is performed using the corresponding function in SASview with imported dq data from SANS data reduction (See Method). As the q^{-2} slope persists beyond the low-q limit of collected SANS datasets, the fitting routine is insensitive to vesicle radii greater than ~70 nm. As shown above by DLS, the hydrodynamic radii of all vesicle samples are >70 nm, therefore an arbitrarily large radius (300 nm) with polydispersity (PD ratio of 0.3 in Schulz distribution) was used to model all SANS patterns presented in Figure 1 a). Solvent scattering length density (SLD) was calculated using known densities and degrees of deuteration, leaving the bilayer scattering length density a the only fitted parameter. The results are in good agreement with experimental SANS patterns shown in Figure 1a). The goodness of fit is measured by the reduced χ^2 value and the small increase for IL-water mixtures can be a consequence of sample aging.

Table S3. Key parameters for modelling SANS patterns, $SLD_{bilayer}$ is the only fitted parameter.

Solvent	$SLD_{bilayer}$ (10^{-6}/Å^2)	$SLD_{solvent}$ (10^{-6}/Å^2)	Volume Fraction (v/v)	Radius (Å)	Thickness (Å)	Reduced χ^2
D_2O	0.64	6.34	0.01	3000	37.4	59
EAF + 50 wt% D_2O	1.52	5.57	0.01	3000	39.9	68
EAF	2.29	5.18	0.01	3000	41.0	19

EtAF + 50 wt% D_2O	1.31	5.84	0.01	3000	40.6	136
EtAF	3.28	6.86	0.01	3000	39.6	36

Modelling of SANS patterns was also done using experimental radii from DLS as shown in Figure S6. The best fits (Figure S6) do not agree well with experimental results at the low-q region. To achieve comparable goodness of fit to Table S3 would require a much higher polydispersity, inconsistent with that observed by DLS (Figure S4). Due to the preparation method used (i.e. the ethanol injection), it is possible that a small fraction of the vesicle population is sufficiently large to dominate the low-q scattering, while a population of smaller sized vesicles of rather well-defined mean size may have led to the weak oscillation at low-q. Therefore, the averaged radii obtained through DLS will not be suitable for SANS modelling

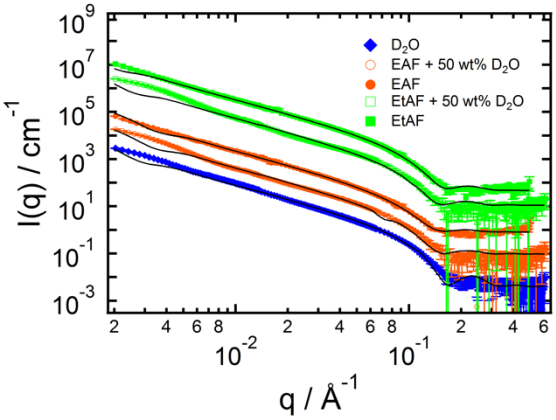

Figure S6. Experimental and calculated (with hydrodynamic radii calculated in Table S1) SANS patterns of 1 wt/v% egg lecithin vesicles in D_2O (blue), and the two PILs ethylammonium formate (EAF, red) and ethanolammonium formate (EtAF, green). SANS patterns in filled markers were collected on D11 beamline; hollow markers denote spectra collected on the QUOKKA beamline approximately 3 months after the NSE studies were completed. SANS patterns were offset for clarity with corresponding modelled pattern shown in solid lines.

Confocal Laser Microscopy:

In aqueous sample, no emission spectrum can be collected from Nile Red due to fluorophore aggregation. This is expected as Nile Red is a known apolar probe and emission is only expected when it is dissolved in apolar environments. Meanwhile, Nile Red in EAF showed pronounced emission at 642 nm upon been excited at 554 nm, confirming EAF is a more apolar solvent relative to water. The emission spectrum of Nile Red partitioned in lipid aggregates in water is sufficiently different to those dissolved in pure EAF, clearly differentiating the two environments. Therefore, if lipid aggregates in EAF are dry, i.e. if negligible solvent molecules are co-assembled into the bilayer, 2 distinct emission spectra are expected from lipid in EAF sample. This is what we observed. Furthermore, the emission spectrum of Nile Red within lipid aggregates was identical for water and EAF solvent, confirming the polarity of hydrocarbon center is independent on solvent, and the center of bilayer must be solvent-free for both water and EAF.

This was further confirmed by fluorescent lifetime imaging. Data were fitted to double exponential decay. The faster decay corresponds to dissolved Nile Red in solvent, which is only significant for the EAF sample, the slower decay corresponds to Nile Red partitioned in lipid aggregates and it is common to both water and EAF samples. A lifetime of around 1.6 ns is calculated for dissolved Nile Red in EAF, while a longer lifetime of 3.4 and 3.3 ns is found for Nile Red in lipid aggregates dispersed in EAF and water respectively. This is consistent with fluorescence emission data and confirms lipid aggregates self-assembled in water or EAF are similar in composition and must be solvent-free.

Surface Tension and DLS Measurements:

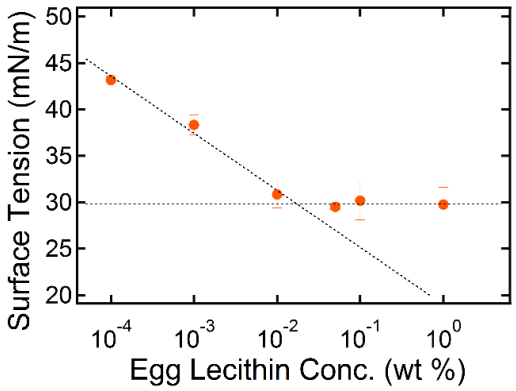

Figure S7. Surface tension profile of egg lecithin in EAF. The solubility limit or critical aggregation concentration of vesicles is determined approx. 0.02 wt%

Table S4. Detection of vesicles by DLS, Y = large aggregates are present, N = instrumental error due to a too low scattering intensity.

Egg Lecithin Conc. (wt%)	water	EAF	EtAF + 10 wt% water[a]
1	Y	Y	Y
0.1	Y	Y	Y
0.01	Y	Y	Y
1 x 10^{-3}	Y	N	N
1 x 10^{-4}	N	----	----

[a] Due to high viscosity of EtAF, 10 wt% water is needed to access the detection limit

Both surface tension measurements (Figure S7) and DLS (Table S3) confirm that the solubility of egg lecithin in ILs should be of the order of magnitude of 10^{-2} wt%, significantly lower than the required 0.9 wt% to account for the observed softness.

References

1. Lindner, P.; Schweins, R., The D11 Small-Angle Scattering Instrument: A New Benchmark for Sans. *Neutron News* **2010**, *21*, 15-18.
2. Wood, K., et al., Quokka, the Pinhole Small-Angle Neutron Scattering Instrument at the Opal Research Reactor, Australia: Design, Performance, Operation and Scientific Highlights. *Journal of Applied Crystallography* **2018**, *51*, 294-314.
3. Farago, B.; Falus, P.; Hoffmann, I.; Gradzielski, M.; Thomas, F.; Gomez, C., The In15 Upgrade. *Neutron News* **2015**, *26*, 15-17.
4. Mezei, F., Neutron Spin-Echo - New Concept in Polarized Thermal-Neutron Techniques. *Zeitschrift Fur Physik* **1972**, *255*, 146-160.
5. Zilman, A. G.; Granek, R., Undulations and Dynamic Structure Factor of Membranes. *Phys. Rev. Lett.* **1996**, *77*, 4788-4791.
6. Nagao, M.; Kelley, E. G.; Ashkar, R.; Bradbury, R.; Butler, P. D., Probing Elastic and Viscous Properties of Phospholipid Bilayers Using Neutron Spin Echo Spectroscopy. *J. Phys. Chem. Lett.* **2017**, *8*, 4679-4684.

7. Gupta, S.; De Mel, J. U.; Schneider, G. J., Dynamics of Liposomes in the Fluid Phase. *Curr. Opin. Colloid Interface Sci.* **2019**, *42*, 121-136.
8. Farago, B.; Monkenbusch, M.; Goecking, K. D.; Richter, D.; Huang, J. S., Dynamics of Microemulsions as Seen by Neutron Spin-Echo. *Physica B-Condensed Matter* **1995**, *213*, 712-717.
9. Hoffmann, I.; Hoffmann, C.; Farago, B.; Prevost, S.; Gradzielski, M., Dynamics of Small Unilamellar Vesicles. *Journal of Chemical Physics* **2018**, *148*.
10. Seifert, U.; Langer, S. A., Viscous Modes of Fluid Bilayer-Membranes. *Europhysics Letters* **1993**, *23*, 71-76.
11. Watson, M. C.; Brown, F. L. H., Interpreting Membrane Scattering Experiments at the Mesoscale: The Contribution of Dissipation within the Bilayer. *Biophysical Journal* **2010**, *98*, L9-L11.
12. Rawicz, W.; Olbrich, K. C.; McIntosh, T.; Needham, D.; Evans, E., Effect of Chain Length and Unsaturation on Elasticity of Lipid Bilayers. *Biophysical Journal* **2000**, *79*, 328-339.
13. SasView Sasview. http://www.sasview.org/ (accessed 06 Feb).